Scientific Research Publishing

American Journal of Plant Sciences, 2026, 17(1), 80-108
https://www.scirp.org/journal/ajps
ISSN Online: 2158-2750
ISSN Print: 2158-2742

Avocado Fruit Defensin (PaDef) Promote Trypsin and Chymotrypsin Enzyme Activity: A Computational Approach

Cinthya Estefani López-Aguilar[1], Karen Astrid Ortiz-Vargas[1], Silvia Valdés-Rodríguez[2], Pedro Navarro-Santos[3], Luis María Suárez-Rodríguez[1], Mariela Gómez-Romero[4], Alejandra Ochoa-Zarzosa[5], Joel Edmundo López-Meza[5], Rodolfo López-Gómez[1]*

[1]Instituto de Investigaciones Químico-Biológicas, Universidad Michoacana de San Nicolás de Hidalgo, Morelia, México
[2]Departamento de Biotecnología y Bioquímica-Centro de Investigación y de Estudios Avanzados del IPN-Unidad Irapuato, Irapuato, México
[3]SECIHTI-Instituto de Investigaciones Químico-Biológicas, Universidad Michoacana de San Nicolas de Hidalgo, Morelia, México
[4]SECIHTI-Facultad de Biología, Universidad Michoacana de San Nicolas de Hidalgo, Morelia, México
[5]Centro Multidisciplinario de Estudios en Biotecnología, Universidad Michoacana de San Nicolás de Hidalgo, Tarímbaro, México
Email: *rodolfo.lopez.gomez@umich.mx

How to cite this paper: López-Aguilar, C.E., Ortiz-Vargas, K.A., Valdés-Rodríguez, S., Navarro-Santos, P., Suárez-Rodríguez, L.M., Gómez-Romero, M., Ochoa-Zarzosa, A., López-Meza, J.E. and López-Gómez, R. (2026) Avocado Fruit Defensin (PaDef) Promote Trypsin and Chymotrypsin Enzyme Activity: A Computational Approach. *American Journal of Plant Sciences*, **17**, 80-108.
https://doi.org/10.4236/ajps.2026.171006

Received: October 26, 2025
Accepted: January 20, 2026
Published: January 23, 2026

Abstract

The fruit ripening process affects the nutritional content and quality. Many fruit species have become more acceptable and present high nutritional value for animal consumption. The avocado is a fruit that produces various compounds of great significance to human nutrition, including peptides crucial to innate immunity. Avocado defensin (PaDef) is an antimicrobial peptide produced during the fruit ripening stage. Defensins have been reported to present antimicrobial activity and act as serin protease inhibitors. However, the present study found that PaDef enhanced the activity of serine proteases (which are digestive enzymes) such as trypsin and chymotrypsin, which is a new finding on the functions of plant defensin. Via the use of molecular docking assessments, the present study found that specific PaDef fragments primarily bind to the active sites of trypsin and chymotrypsin. Moreover, the stability and behavior of the peptides generated *in silico* from PaDef were evaluated in the presence of chymotrypsin A protease digestion using molecular dynamics simulations under basic conditions. The results obtained suggest that the selective fragments of PaDef peptides induce enzyme activity via allosteric modulation, an area of increasing research interest due to its implications for both fundamental biochemistry and applied biotechnology. The present study is a

novel report on the activity of a plant defensin at a molecular level.

Keywords

Antimicrobial Peptides, Avocado, Computational Modeling, Defensin PaDef, Molecular Dynamics, Protease Activity

1. Introduction

Over the course of their evolution, plants develop a fruit architecture which protects their seeds from the natural environment as part of a reproduction strategy that increases dispersal by making fruit more attractive to fauna as a source of both energy and nutrition [1]. Plants and other organisms produce antimicrobial peptides (AMPs), which function as a defense mechanism against pathogens, playing a crucial role in innate immunity in both plants and animals [2]. Their small (<10 kDa) molecule size, which is mainly cationic and amphipathic, promotes the interaction between the AMP and the target membrane [3]. Plant defensins comprise a significant proportion of the AMPs, while their amino acid composition, which consists of 45 - 54 amino acids and ~5 kDa, is indicative of their unique molecular characteristics. Plant defensins are also known for their high degree of basicity and their use of 8 - 10 cysteines to form the disulfide bridges that stabilize their structures. Studies conducted on their three-dimensional structure have shown that it comprises a triple-stranded β-sheet with an α-helix in parallel. These defensins can be expressed during storage and reproduction and have been associated with antibacterial and antifungal activities [3]. In addition, various plant defensins have been reported to inhibit α-amylase, trypsin, the sodium channel, and protein synthesis [4]-[6]. The literature reports a defensin obtained from *Cassia festula* seeds exerting an inhibition effect on the enzyme trypsin [7]. The avocado contains AMPs such as defensins and snakins. The PaDef defensin gene is abundantly expressed in the fruit of the native Mexican variety of avocado (*Persea americana* var. drymifolia) and has been shown both to exhibit antibacterial activity and cytotoxicity against several human cancer cell lines [8] [9] and to function as an epigenetic regulator [10]. Present in all kingdoms, proteases catalyze the hydrolysis of peptide bonds, thereby generating shorter chains of amino acid residues [11], and regulating multiple physiological and pathological processes [12] [13]. Serine proteases are one of the most abundant groups of proteolytic enzymes and contain, in their active center, three conserved amino acid residues, Histidine (His), Aspartic acid (Asp), and Serine (Ser), with the latter occupying the central region [14] [15]. Trypsin and chymotrypsin are representative of serine proteases, which, in animals, participate in nutrition, blood coagulation, fibrinolysis, and cell development. Plants modulate various physiological processes, including cell growth, senescence, and pollen formation, presenting defensive mechanisms that protect against biotic stresses, pests, and phytopatho-

genic microorganisms [14] [16]. Given their importance for organism development, the regulation of proteases is vital to maintaining homeostasis and ensuring survival [17]-[19]. Bioactive peptides are released during both the enzymatic proteolysis (as seen in gastrointestinal digestion and *in vitro* hydrolysis using proteolytic enzymes) of proteins and food processing (cooking, fermentation, and ripening). Bioactive peptides are mainly known for inhibiting protein-protein interactions due to their small size and specificity [20]. A new emerging approach to drug design is based on secondary binding site effects. In this approach, small molecules can bind into secondary binding sites on the targeted biomolecules rather than the main orthosteric sites. These secondary sites are called allosteric sites. A molecule capable of binding to an allosteric site and remotely altering (or modifying) the conformation of the primary orthosteric binding site of the biological target is known as an allosteric modulator [21]. In this work, we report experimental evidence that PaDef induces the serine proteases trypsin and chymotrypsin activity. To give insights into the interactions and stability of the PaDef peptide against the proteases, molecular docking assessments and molecular dynamics simulations between the PaDef peptide and trypsin and chymotrypsin proteases were studied.

2. Materials and Methods

2.1. *In Vitro* PaDef Serine Protease Assay

The synthetic PaDef used by the present study, which presented a purity level of 85% - 95% (as established via HPLC) was obtained from BIOMATIK as a lyophilized water-soluble powder. The PaDef was then dissolved in a 20% DMSO solution to facilitate the formation of disulfide bridges within the peptide. Trypsin and chymotrypsin activity assays were performed following the modified Erlanger method [22] to evaluate the effect of the PaDef enzyme activity, using Nα-benzoyl-DL-arginine-p-nitroanilide (BApNA; Sigma) as a substrate. The assay used 50 µg/ml of bovine trypsin and chymotrypsin (Sigma) separately and then mixed with 125 µl of Tris-HCl (100 mM, pH = 8), with the solutions subject to incubation at 37˚C for 15 min with different PaDef concentrations (0.05, 0.5, 5, and 50 µg/ml). For positive inhibition control, tepary bean protease inhibitor (TBPI) [23] was used at a concentration of 6 µg/ml, with 20% dimethylsulfoxide (DMSO) used as the peptide vehicle. Subsequently, 20 µl of BApNA at 10 mM was added, with incubation for 15 min then applied to facilitate the reaction. The reaction was terminated by adding 30% acetic acid (20 µl), with the optical density then measured at 410 nm. The reactions were carried out in triplicate at three distinct points in the experiment. The data obtained were analyzed using the non-parametric Kruskal-Wallis test, with multiple comparisons using non parametric Dunnett's test with the JMP and R statistical packages.

2.2. Trypsin and Chymotrypsin Molecular Docking

The molecular docking assessments used the PaDef peptide (47aa) (Genbank

AGC82207.1) as the ligand, which was subject to molecular modeling using the SWISS MODEL online tool [24] and was selected due to its structural homology with plant defensin-type peptides (SMTL ID: 7c2p.1), with the corresponding FASTA sequence then generated. Acknowledge that predicting cleavage sites with the PeptideCutter tool [25] is an *in silico* assumption to determine how the PaDef was cleaved by both enzymes studied. The molecular structures of the serine proteases chymotrypsin A (PDB ID: 1T8L) and trypsin (PDB ID: 3BTH) were obtained from the RCSB PDB database [26] at resolutions of 1.75 and 1.75 Å, respectively.

The proteases were then prepared by adding the missing hydrogens and assigning Kollman charges using both Chimera and AutoDockTools [27] [28]. Blind molecular docking was also carried out via the use of AutoDock CrankPep [29], with the entire proteins and a padding of 4 Å entered as parameters into the search box, with the peptide sequence also provided so that the best helical or extended conformation could be determined for each of the peptides in each protease. The docking calculations for the PaDef peptide sequence were performed for 100 independent searches and three million evaluations of the scoring functions. Once the best conformations for the peptides had been obtained, the Discovery Studio BIOVIA program [30] was used for visualization and analysis, with the favorable and unfavorable interactions between each of the peptides and the receptor in the different regions then identified and analyzed. Moreover, molecular docking calculations were conducted for the positive control, BApNA, against both serine proteases in order to correlate the results obtained with the *in vitro* assay.

2.3. Molecular Dynamics Simulations for the Chymotrypsin A PaDef Peptides

To determine the stability of the PaDef peptides and their interaction with chymotrypsin A at pH 8, the NAMD software [31] was used, with the initial conformation of the peptides for the molecular dynamic simulations selected from the best-predicted pose for each peptide, as obtained from the molecular docking assessments. The parameterization and preparation of the complexes were conducted based on the Solution Builder module using the CHARMM-GUI platform [32] [33], with a pH = 8 and a rectangular cell of 74 × 74 × 74 $Å^3$, while solvation was carried out via a TIP3P water model [34] and neutralization achieved by adding Na^+ and Cl^- ions at a concentration of 0.15 M. The forcefield used for the simulations was CHARMM36m, which has been employed successfully by previous studies to simulate peptide-protein complexes [35]. Long-range electrostatic interactions were modeled using the particle mesh ewald (PME) method [36] and a 12 Å cutoff for non-bonded interactions. The molecular dynamics simulations were carried out in four stages. Firstly, energy minimization was performed with a conjugate gradient algorithm [37] for 100,000 interaction steps with a time-step of 1.0 *fs*. Then, the NVT ensemble was generated by heating the system from 0 to

310 K at 1 K intervals for a period of 500 *ps* and then maintaining the temperature at 310 K for a period of 500 *ps*, via the use of the Langevin thermostat. Subsequently, thermal equilibrium was achieved for the NPT ensemble at 1 atm and 310 K for 5 *ns* using the Langevin thermostat and the Nosé-Hoover Langevin piston barostat model [38] [39], with, finally, the NPT ensemble then used for 100 *ns* with a time-step of 2.0 *fs*. The trajectories of the molecular dynamic simulations were post-processed using the VMD program [40] to calculate both the root mean square deviation (RMSD) values and the hydrogen bond interactions presented between the peptides and the receptor. The MMGBSA (molecular mechanics/generalized born surface area) and MMPBSA (molecular mechanics/poisson-boltzmann surface area) methods are useful approaches for helping estimate the Gibbs free energy value [41]. Although both methods can predict the Gibbs free energy of ligands and macromolecules, the MMPBSA is more effective for use with small peptides, while the MMGBSA is more suitable for studying the interaction between medium-sized peptides and proteins [42]. Therefore, the present study calculated the binding free energies for each complex using the MMGBSA via the gmxMM/PBSA tool [43], integrating the last 50 *ns* obtained from the production stage of the molecular dynamic simulations, and exploring an average of 500 snapshots.

3. Results and Discussion

3.1. *In Vitro* PaDef Serine Protease Assays

Trypsin and chymotrypsin A activity assays were performed to evaluate the effects of PaDef on the activity of the enzymes of interest, using Nα-benzoyl-DL-arginine-p-nitroanilide BApNA as a substrate. The assays were carried out using the chemically synthesized PaDef peptide at four concentrations (0.05, 0.5, 5, and 50 µg/ml). Defining a unit of enzymatic activity as the enzyme required to degrade 3.2 µM of BApNA/min enabled the analysis conducted to determine the possible effect of PaDef on protease activity. While the PaDef did not show an inhibitory effect on serine protease activity, it did promote the activity. In both enzymes analyzed, the enzymatic activity increased in line with the PaDef peptide concentration. Trypsin activity increased by approximately 30% at a concentration of 50 µg/ml, while chymotrypsin activity increased by approximately 150% at a concentration of 5 µg/ml. The increase in protease activity was higher for chymotrypsin than for trypsin (**Figure 1(a)**, **Figure 1(b)**). Applied after Dunnett's multiple comparisons test, the non-parametric Kruskal-Wallis test showed a significant difference of $X^2 = 30.23$ ($P > 0.0001$) for trypsin and $X^2 = 30.65$ ($P > 0.0001$) for chymotrypsin A for the PaDef treatments applied, except for the results of the comparison between the control group and 0.05 µg/ml PaDef. It is important to note that, for the experiments conducted with both trypsin and chymotrypsin A, the vehicle (DMSO 20%) did not generate any change in the activity of the enzymes (**Figure 1(a)** and **Figure 1(b)**).

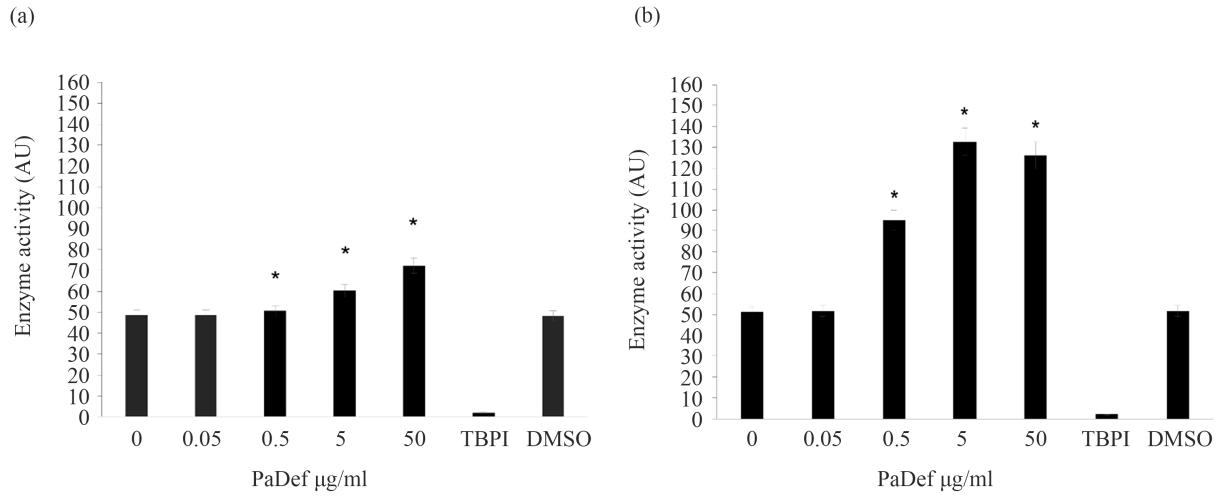

Figure 1. Effect of PaDef on serine protease enzymatic activity: (a) Trypsin and (b) Chymotrypsin A; both enzymes analyzed showed an increase in activity in a manner that depended on the concentration of the peptide; the Kruskal-Wallis test showed a significant difference* compared to the control ($P < 0.0001$).

3.2. Molecular Docking of PaDef Peptides on Chymotrypsin A and Trypsin

While the experimental results obtained by the present study provide valuable insights into enzymatic behavior, they do not reveal the detailed atomic-level mechanisms that would further elucidate its *in vitro* findings for serine proteases. Computational methods, including molecular dynamics simulations and molecular docking assessments, offer powerful tools to bridge the gap in the results described above. As these methods enable the in-depth exploration of conformational changes, interaction energies, and allosteric effects that are all difficult to capture experimentally, computational techniques were used to examine the molecular mechanisms underlying the observed increase in chymotrypsin activity, with the aim of identifying the key structural and energetic factors responsible for this enhancement. The catalytic regions of chymotrypsin A (cr_C) and trypsin (cr_T) are well-known and well-studied sites, comprising the catalytic triad (His57, Asp102, and Ser195) [44]-[47]. However, other interactions have been observed by other *in silico* studies conducted on chymotrypsin A [48], in which ligand structures not only interacted with the catalytic triad but also entered the hydrophobic cavity of the binding pocket. Said interactions involved Leu160, Gly184, Ser189, Ser190, Cys191, Met192, Val213, Gly216, Ser217, Cys220, Ser221, Thr224, Gly226, and Tyr228. Furthermore, hydrogen bond interaction with both the known inhibitors and the amino acids His57, Tyr146, Gly193, Gly216, and Ser218 at the active site was revealed by the molecular docking studies conducted [49]. To correlate the results presented in this section, the positive control BApNA was analyzed computationally by means of molecular docking assessments conducted on both chymotrypsin A and trypsin, obtaining scoring energies of −8.9 and −8.6 kcal/mol, respectively. The best conformation was found in the catalytic region of each serine protease, whose interaction maps can be found in **Figure S1** of the

Supplementary Material section. Given the high level of activity observed for the PaDef peptide in these proteases, as shown in **Figure 1**, it was hypothesized that the peptide would be susceptible to breakdown by these enzymes. The online tool PeptideCutter [24] was used to cleave the PaDef peptide in the presence of the enzymes of interest. The results obtained confirmed that chymotrypsin A cleaves the PaDef peptide into three fragments (namely, p1, p2, and p3), as shown in **Figure 2(a)**. Meanwhile, trypsin was observed to cleave the peptide into six fragments (namely, p4, p5, p6, p7, p8, and p9) (**Figure 3(a)**). Once the fragments had been identified, the docking assessments were performed for each peptide sequence and each protease. Subsequently, the favorable and unfavorable interactions between

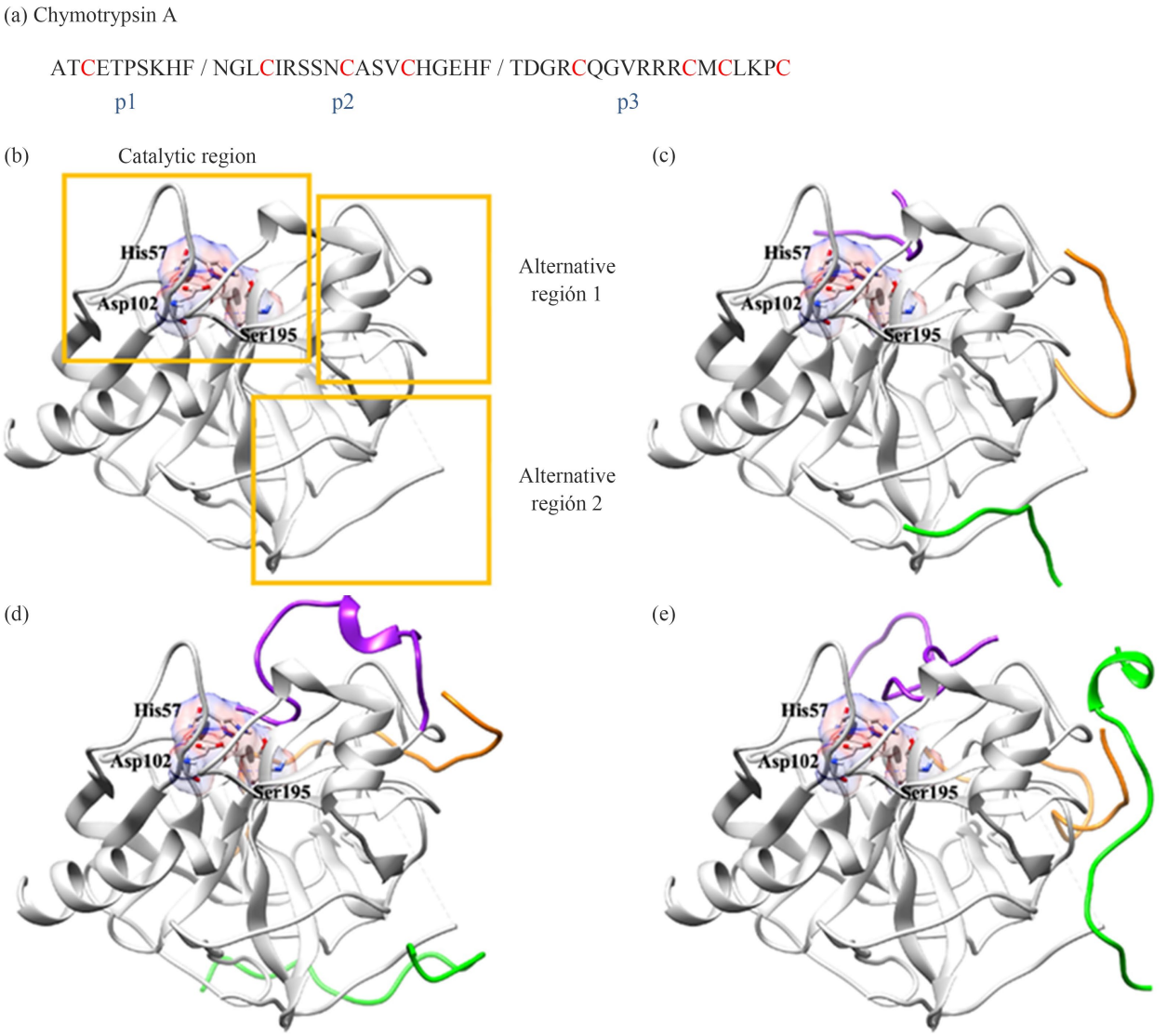

Figure 2. The most affine conformations for the PaDef peptides against chymotrypsin A, with peptides p1, p2, and p3 docked on chymotrypsin A: (a) PaDef peptide sequences (p1-p3) generated by chymotrypsin A protease activity; (b) the orange box shows the main three regions found for chymotrypsin A; (c)-(e) show the best conformations of p1, p2, and p3, respectively, found for each region, with the peptides in purple docked near the catalytic region and the peptides in orange docked near Alternative Region 1, while the peptide docked on Alternative Region 2 is in green.

each of the peptides and the receptor in the different regions were obtained using the Discovery Studio program (BIOVIA) [30]. The analysis carried out on the ten best conformations of the 100 obtained from the molecular docking calculations conducted on the peptides, for chymotrypsin A revealed that eight of the ten poses for Peptide 1 (p1) were found in the cr_C catalytic region. The others were found in the alternative regions 1 (arC_1) and 2 (arC_2), which may be allosteric regions given the increased serine protease activity observed in the experimental data (**Figure 2(b)**). Erlanger *et al.* [50] [51] performed research on three substrates, finding that chymotrypsin A has an additional functionally-important binding site to the active site of the catalytic triad, namely a hydrophobic allosteric site that may improve the activity of the enzyme and is located near the catalytic site without causing steric problems. This would mean that the alternative sites considered in this study, arC_1 and arC_2 as identified by the molecular docking assessment, may be allosteric sites that accelerate activity and present a considerable number of hydrophobic and hydrogen bonding interactions. For Peptide 2 (p2), seven poses were docked on cr_C, one on arC_1, and two on arC_2. Finally, for Peptide 3 (p3), four of the ten poses were docked on cr_C, two were docked on arC_1, one on arC_2, and three on other regions. The best binding energies and the best conformation at each site are summarized in **Table 1** and parts (c) - (e) of **Figure 2**, respectively. The best affinity energy value for p1 and p2 was obtained at the cr_C site of chymotrypsin A and at arC_1 for p3. The order for affinity energy values found for the cleaved peptides was p2 < p3 < p1. It may be that p2 presents the best energy affinity, because it contains more amino acids that allow it to interact strongly with the protease.

Table 1. Scoring energies (kcal/mol) for p1, p2, and p3, as docked on the cr_C, arC_1, and arC_2 regions of chymotrypsin A.

Peptide	Scoring energies (kcal/mol)		
	cr_C	arC_1	arC_2
p1	−17.6	−16.3	−15.6
p2	−25.6	−22.4	−20.6
p3	−18.6	−19.5	−17.9

To correlate the affinity energies presented in **Table 1**, the favorable and unfavorable interactions between each peptide and the cr C, arC_1, and arC_2 regions of the enzyme were determined and are shown in **Tables S1-S9**. These results show that the three peptides interacted with the Ser195 residue when docked on cr_C. For the allosteric site arC_1, the amino acids Asn18, Thr144, and Arg145 interacted with the three peptides, while the amino acids Gly19, Glu20, Glu21, Thr37, Gln73, Asn150, Asp153, Arg154, Gln156, and Thr222 interacted with two peptides. Finally, for the allosteric site arC_2, the amino acid Leu10 interacted with all three peptides and the amino acids Val9, Thr135, and Lys202 interacted with just two peptides. In addition, the following interactions were observed for

p1 when docked on cr_C: one salt bridge interaction; nine hydrogen bond interactions (with the amino acids Asp35, Phe41, Cys42, Gly193, Ser195, and Gly216); one carbon-hydrogen bond interaction; two electrostatic π-cation interactions; four hydrophobic interactions (π-σ, π-π stacked, alkyl, and π-alkyl); and one π-sulfur interaction. The present study found the following for p1 docked to the arC_1: one salt bridge interaction; one electrostatic attractive charge interaction; seven hydrogen bond interactions (with amino acids Ser11, Asn18, Glu21, Thr144, Gln156, and Thr222); two carbon-hydrogen bond interactions; two hydrophobic π-alkyl interactions; and one unfavorable donor-donor interaction. For p1 docked to the arC_2, the following was found: one salt bridge interaction; one attractive charge electrostatic interaction; four hydrogen bond interactions (with the amino acids Pro8, Leu10, and Thr135); one carbon-hydrogen interaction; one π-donor hydrogen bond interaction; two hydrophobic alkyl interactions; one unfavorable acceptor-acceptor interaction; and one unfavorable bump interaction. For p2 docked on cr_C, one electrostatic attractive charge interaction, thirteen hydrogen bond interactions (with the amino acids His57, Cys58, Tyr146, Lys170, Tyr171, Ser195, Ser217, Ser218, and Thr219), four carbon-hydrogen bond interactions, and five hydrophobic interactions (two alkyls and three π-alkyl). For p2 docked on arC_1, the following was found: one salt bridge interaction; two electrostatic attractive charge interactions; twelve hydrogen bond interactions (with the amino acids Asn18, Gly19 twice, Thr37, Ile80, Thr144, Asn150, Thr151 twice, Asp153 twice, and Thr222); five carbon-hydrogen bond interactions; one π-donor hydrogen bond interaction; two hydrophobic interactions (π-σ and π-alkyl, respectively); and three unfavorable interactions due to unfavorable bump, unfavorable positive-positive, and unfavorable donor-donor interactions. For p2 docked to the arC_2, the present study found the following: one salt bridge interaction; two attractive charge electrostatic interactions; eight hydrogen bond interactions (with the amino acids Gln7, Leu10, Ser113, Phe114, Gln116, and Thr117); ten hydrophobic interactions (π-σ, π-π T-shaped, six alkyl, and two π-alkyl); one π-lone pair interaction; and one unfavorable donor-donor interaction. For p3 docked the cr_C, the present study found the following: three salt bridge interactions; two electrostatic attractive charge interactions; eight hydrogen bond interactions (with the amino acids His40, Gly59, Ser96, Leu97, Ser195, and Ser218); two electrostatic π-cation interactions; and six hydrophobic interactions (three alkyls and three π-alkyl). For p3 docked to the arC_1, the present study found the following: five salt bridge interactions; four electrostatic attractive charge interactions; eleven hydrogen bond interactions (with the amino acids Asn18 twice, Glu21, Thr37 twice, Gln73, Thr144, Asn150, Asp153, Arg154, and Gln156), one carbon-hydrogen bond interaction; one hydrophobic alkyl interaction; and four unfavorable interactions due to unfavorable bump, two to unfavorable donor-donor, and one to unfavorable acceptor-acceptor interactions. For p3 docked to the arC_2, the following was found: one salt bridge interaction; one electrostatic attractive charge interaction; eight hydrogen bond interactions (with the amino acids Asn18,

Ser159, Ser186, Thr219, Cys220, and Thr222); three carbon-hydrogen bond interactions; and four hydrophobic alkyl interactions. The six fragments that were cleaved due to trypsin activity are shown in Figure 3(a). For peptides 4 (p4), 5 (p5), 7 (p7), and 9 (p9), the ten best conformations only recognized the known catalytic region of trypsin (cr_T) without identifying any conformers in alternative regions. For Peptide 6 (p6), six of the ten poses were found in the cr_T and four were found in an alternative region (ar_T), while, for peptide 8 (p8), only one of the first ten poses was found in the cr_T, probably because of its small size. The best conformations for each peptide are shown in Figure 3(b), with the best binding energies at each site summarized in Table 2.

a) Trypsin

ATCETPSK / HFNGLCIR / SSNCASVCHGEHFTDGR / CQGVR / RR / CMCLKPC
p4 p5 p6 p7 p8 p9

b)

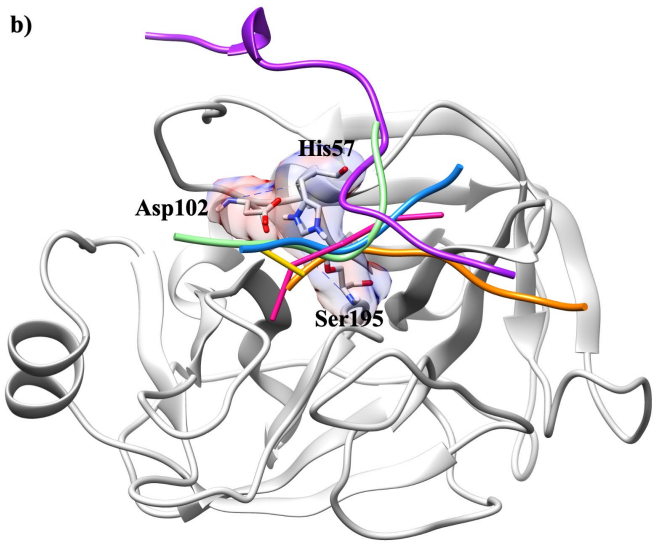

Figure 3. The most affine conformations for the PaDef peptides against trypsin, with peptides p4, p5, p6, p7, p8, and p9 docked against trypsin: a) PaDef peptide sequences (p4-p9) generated by trypsin protease activity; b) The best docked conformations in the catalytic region, with the colors green, orange, purple, magenta, yellow, and blue representing p4, p5, p6, p7, p8, and p9, respectively.

The order for affinity energy values for PaDef peptides cleaved in the presence of trypsin, at the cr_T site, was p6 < p5 < p9 < p4 < p7 < p8. Peptide p6 also presented a scoring energy in the ar_T of −20.2 kcal/mol, a lower affinity than that observed for p6 in the cr_T. It should be noted that p5 and p6 present most of the amino acids constituting p2 observed for the chymotrypsin cleavage. Comparing the fragmented peptides' binding energies for chymotrypsin and trypsin in their respective catalytic regions reveals that the best binding energy presented by p2 was for chymotrypsin, followed by trypsin for p6, chymotrypsin for p3 and p1, and, finally, trypsin for p5. These results suggest that all three PaDef fragments—

p1, p2, and p3—may enhance chymotrypsin activity. However, only one PaDef fragment (p6) activated trypsin, which may explain the experimental findings of the present study, which show p2 presenting the best affinity energy. Notably, the affinity observed for the p1-p3 fragments for the allosteric chymotrypsin sites (see Table 1) was sometimes higher than the affinity observed for p6 for the catalytic site. This may explain why higher levels of chymotrypsin enzymatic activity than trypsin activity was observed, even at lower concentrations. Furthermore, the affinity energies presented in Table 2 are related to the favorable and unfavorable interactions between each peptide docked on cr_T, interactions shown in Tables S10-S15. These results show that p4, p5, p7, and p9 interact with the amino acids His57 and Ser195, while p6 and p8 only interact with the amino acid His57.

Table 2. Scoring energies (kcal/mol) for p4-p9, as docked on the cr_T region of trypsin.

Peptide	Scoring energies (kcal/mol)
	cr_T
p4	−13.4
p5	−17.5
p6	−20.6
p7	−13.3
p8	−6.5
p9	−13.9

A comparison of the scoring energies presented in Table 1 and Table 2 with the scoring energies obtained for the positive control reveals that almost all the peptides have a better affinity in the catalytic region for both chymotrypsin A and trypsin than for BApNA.

3.3. Basic Conditions for Molecular Dynamics Simulations Conducted with Chymotrypsin A

Following the identification of the PaDef fragment complexes as well as the protease that exhibited the highest level of activity (chymotrypsin A), the present study then explored their stability over time using molecular dynamics simulations. The corresponding molecular dynamics properties were obtained from the last 100 *ns* of the production stage. According to the RMS deviations, in most cases, the peptides remained stabilized throughout the simulation trajectory. It is important to highlight that trypsin and chymotrypsin A are digestive enzymes present in the digestive system under basic media conditions (pH = 8), which were the conditions applied during the simulations conducted by the present study. Figure 4 shows the RMSD values obtained for the peptides and proteases studied. According to Figure 4(a), p1 exhibited more significant fluctuations in the simulation, stabilizing at an average RMSD of 5.2 Å, as shown in Table 3. In contrast, p2 stabilized after approximately 10 *ns* and then exhibited some fluctuations, while appearing to be more stable in the last 40 *ns*. Similarly, p3 seemed to be

stable throughout the simulation. All of the peptides did not present diffusion. The RMSD values obtained for the proteases (Figure 4(b)) show that, for the three peptides, chymotrypsin A was stable throughout the simulation and even more stable when p2 and p3 were complexed than in the presence of p1. This finding is verified by the values presented in Table 3, which shows average RMSD values for the protease of 1.6 Å, 1.7 Å and 1.9 Å, for p2, p3, and p1, respectively. Moreover, when the alternative regions of chymotrypsin A were explored for each peptide, almost all the peptides failed to stabilize, with only p2 at arC_2 presenting partial stabilization during the simulation.

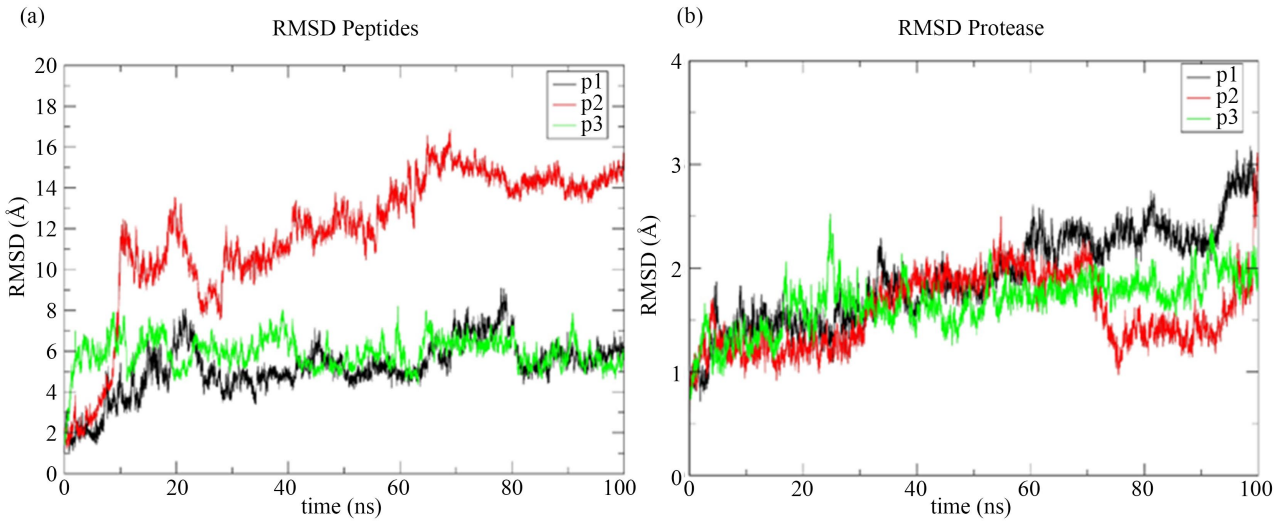

Figure 4. RMSD (in Å) of the peptides: (a) p1, p2, and p3; and (b) Chymotrypsin A during the production stage.

Table 3. Average RMSD values (in Å) for both chymotrypsin A and the peptide aligned to the protease.

Peptide	Region	RMSD Protease	RMSD Peptide
p1	cr_C	1.923	5.175
p2	cr_C	1.578	11.720
p3	cr_C	1.671	5.915

3.4. Hydrogen Bond Analysis and MMGBSA Binding Free Energy Calculations

In order to identify hydrogen bonds exhibiting moderate to strong strength, it is first necessary to establish a range of interatomic distances, which, in the case of the present study, corresponded to 1.8 - 3.2 Å. These distances were monitored for the entire simulation period and then used to identify the hydrogen bond interactions that occurred during that period. During such a simulation, when the occupancy percentage exceeds 100%, the protease and the peptide residues may interact with more than one hydrogen bond. The H-bond occupancy, defined as the period of time (expressed as a percentage) for which an H-bond is present in

a simulation, is reported in Table 4. An H-bond occupancy of over 10 % was selected for the production stage of each simulation.

Table 4. Hydrogen bond occupancy higher than 10 %, as calculated during the 100 *ns* simulations.

Peptide	Region	Hydrogen bonds sorted	Donor	Acceptor	% Occupancy
p1	cr_C	8	LYS36-Side	p1_PHE10-Side	84.86%
			p1_LYS8-Side	ASP64-Side	138.72%
			p1_HSD9-Main	ASP35-Side	74.04%
			p1_HSD9-Side	ASP35-Side	50.16%
			LYS36-Side	p1_PHE10-Main	13.46%
			p1_THR5-Side	HSD57-Main	14.36%
			p1_LYS8-Side	GLY59-Main	60.72%
			LYS36-Side	p1_HSD9-Main	11.60%
p2	cr_C	13	p2_ARG6-Side	GLY216-Main	11.36%
			LYS175-Side	p2_SER8-Main	31.83%
			LYS175-Side	p2_ALA11-Main	20.67%
			p2_HSD15-Side	GLY216-Main	12.97%
			LYS175-Side	p2_ASN9-Main	10.38%
			p2_SER7-Main	LEU97-Main	12.46%
			LYS175-Side	p2_SER12-Main	37.39%
			LYS175-Side	p2_VAL13-Main	28.81%
			LYS175-Side	p2_HSD15-Side	69.41%
			SER218-Main	p2_HSD15-Main	51.88%
			p2_ASN1-Main	ASP35-Side	11.62%
			p2_CYS4-Main	HSD57-Main	13.95%
			SER218-Side	p2_GLU17-Main	11.80%
p3	cr_C	15	THR151-Side	p3_ARG11-Main	13.74%
			p3_ARG10-Side	PHE39-Main	16.78%
			p3_ARG10-Side	HSD40-Main	40.90%
			p3_ARG10-Side	ASP35-Side	72.14%
			p3_ARG9-Side	CYS58-Main	57.52%
			GLY216-Main	p3_GLN6-Side	32.80%
			SER76-Side	p3_CYS18-Side	19.36%
			LYS82-Side	p3_CYS18-Side	28.72%
			p3_LYS16-Main	GLN73-Main	20.64%
			p3_LYS16-Side	SER75-Main	16.96%
			p3_LYS16-Side	GLU70-Side	147.96%
			p3_GLN6-Side	GLY216-Main	14.62%
			p3_LYS16-Side	ASP72-Main	45.56%
			p3_LEU15-Main	GLN73-Main	34.92%
			LYS175-Side	p3_ASP2-Side	19.04%

Table 4 shows that, during the simulation conducted for Peptide p1, eight hydrogen bond interactions presented an H-bond occupancy of over ten percent. Furthermore, the most significant interactions observed for p1 were with the Asp35, Lys36, Asp64, and Gly59 pertaining to chymotrypsin A. Although p1 exhibits an interaction with His57, its occupancy percentage was not as high. A higher number of hydrogen bond interactions were observed for p2 than for p1, while two interactions with percentages higher than 50 % were observed for p2_His15, as well as the amino acids Lys175 and Ser218. Moreover, one interaction was observed between the amino acid His57 and the cysteine of p2, specifically Cys4. For p3, Table 4 shows more interactions of over ten percent than those observed for p1 and p2, while the most significant interactions were with the amino acids Asp35, Cys58, and Glu70. It should be noted that two interactions were observed between p3_Cys18 and the amino acids Ser76 and Lys82. Additionally, the evaluation of the stability of p2 in arC_2 revealed some interactions of over 50 % with Glu20, Asp72, and Lys202, which gave it partial stability in this region during the simulation. Finally, the binding free energy was calculated using the MMGBSA model for the final 50 *ns* of the simulation, yielding the results presented in Table 5. It can be concluded that, under basic conditions, p3 most strongly promotes the stability of peptides in the cr_C, followed by p2 and p1. Furthermore, the electrostatic interactions were observed to contribute more to the binding free energy than van der Waals interactions, with the former/latter interactions important for the stability of the peptides and their affinity to the protease.

Table 5. MMGBSA binding free energy (kcal/mol) for the complexes of each peptide for chymotrypsin A.

Peptide	ΔG Van der Waals	ΔG electrostatic	ΔG
p1	−36.08	−172.88	−37.44
p2	−57.33	−154.98	−44.09
p3	−75.12	−272.08	−53.17

While studies of defensins acting as enzyme activators do not appear in the literature, there is one report of an LTP-type antimicrobial peptide participating in the polygalacturonase-mediated pectin degradation of the polygalacturonase in tomato fruit during the ripening process [52]. Several plant defensins have been reported, like protease inhibitors; one defensin from *Cassia fistula* showed activity as a trypsin inhibitor, the authors proposed that this activity was due to a lysine residue on position 25 [7]. Cowpea defensin inhibits trypsin, but not chymotrypsin A; the final model generated by docking concludes that a lysine residue at position 11 occupies the S1 specificity pocket of trypsin [53]. PaDef sequence lacks the two lysins present in the sequence of the aforementioned defensins. Both reports were carried out with defensins isolated from plant tissues, and the models were carried out with the complete sequence of defensins. Our *in silico* work was

done with theoretical peptides generated by the action of the proteases on PaDef; the peptides generated by the action of these digestive enzymes on other defensins probably generate fragments of different sizes and sequences. The difference in activity observed in this work concerning the two digestive proteases could be a consequence of the different peptides generated by Trypsin and Chymotrypsin digestion on PaDef. Chymotrypsin A is digestive enzyme found under basic (pH = 8) conditions in the digestive system. The behavior of the peptides generated by dynamics simulations (please see the RMSD analysis) shows that pH 8 favored the interaction of three peptides with the three regions of the chymotrypsin (cr_C, arC_1, and arC_2). Our theoretical results would explain what was observed with the increase in protease activity under experimental conditions and propose that PaDef has an allosteric influence on the serin proteases trypsin and chymotrypsin A activity. However these are putative sites and computational results provide a strong hypothesis for the activation mechanism, which would require future experimental validation such as site-directed mutagenesis.

4. Conclusion

In vitro, PaDef induces serine protease activity. Using computational docking, the present study found three energetically-favorable union sites between chymotrypsin A and the peptides generated by the protease activity of interest and only one such site for trypsin. Using molecular dynamics simulations, the present study found that the three peptides generated by chymotrypsin A under basic environmental conditions promote peptide stability with low RMSD values and favorable hydrogen bond interactions. The results obtained suggest that antimicrobial PaDef peptides exert an allosteric effect on serine protease activity, a novel finding for the activity of an antimicrobial plant peptide.

Acknowledgements

We express our appreciation to the Consejo Nacional de Humanidades, Ciencias y Tecnologías (CONAHCYT) for Cinthya Estefany López Aguilar scholarship and UMSNH Coordinación de la Investigación Científica.

Conflicts of Interest

The authors declare no conflict of interest.

References

[1] Hiwasa-Tanase, K. and Ezura, H. (2014) Climacteric and Non-Climacteric Ripening. In: Paravendra, N., Bouzayen, M., Mattoo, A.K. and Pech C., Eds., *Fruit Ripening*: *Physiology*, *Signalling and Genomics*, CABI, 1-14. https://doi.org/10.1079/9781845939625.0001

[2] Sher Khan, R., Iqbal, A., Malak, R., Shehryar, K., Attia, S., Ahmed, T., *et al.* (2019) Plant Defensins: Types, Mechanism of Action and Prospects of Genetic Engineering for Enhanced Disease Resistance in Plants. *3 Biotech*, **9**, Article No. 192. https://doi.org/10.1007/s13205-019-1725-5

[3] Meneguetti, B.T., Machado, L.S., Oshiro, K.G.N., Nogueira, M.L., Carvalho, C.M.E. and Franco, O.L. (2017) Antimicrobial Peptides from Fruits and Their Potential Use as Biotechnological Tools—A Review and Outlook. *Frontiers in Microbiology*, **7**, Article ID: 2136. https://doi.org/10.3389/fmicb.2016.02136

[4] Liu, Y., Cheng, C., Lai, S., Hsu, M., Chen, C. and Lyu, P. (2006) Solution Structure of the Plant Defensin Vrd1 from Mung Bean and Its Possible Role in Insecticidal Activity against Bruchids. *Proteins*: *Structure*, *Function*, *and Bioinformatics*, **63**, 777-786. https://doi.org/10.1002/prot.20962

[5] Stotz, H.U., Thomson, J. and Wang, Y. (2009) Plant Defensins: Defense, Development and Application. *Plant Signaling & Behavior*, **4**, 1010-1012. https://doi.org/10.4161/psb.4.11.9755

[6] Parisi, M.G., Ozón, B., Vera González, S.M., García-Pardo, J. and Obregón, W.D. (2024) Plant Protease Inhibitors as Emerging Antimicrobial Peptide Agents: A Comprehensive Review. *Pharmaceutics*, **16**, Article 582. https://doi.org/10.3390/pharmaceutics16050582

[7] Wijaya, R., Neumann, G.M., Condron, R., Hughes, A.B. and Polya, G.M. (2000) Defense Proteins from Seed of Cassia Fistula Include a Lipid Transfer Protein Homologue and a Protease Inhibitory Plant Defensin. *Plant Science*, **159**, 243-255. https://doi.org/10.1016/s0168-9452(00)00348-4

[8] Guzmán-Rodríguez, J.J., López-Gómez, R., Suárez-Rodríguez, L.M., Salgado-Garciglia, R., Rodríguez-Zapata, L.C., Ochoa-Zarzosa, A., *et al.* (2013) Antibacterial Activity of Defensin PaDef from Avocado Fruit (Persea Americana var. Drymifolia) Expressed in Endothelial Cells Against *Escherichia coli* and *Staphylococcus aureus*. *BioMed Research International*, **2013**, Article ID: 986273. https://doi.org/10.1155/2013/986273

[9] Flores-Alvarez, L.J., Guzmán-Rodríguez, J.J., López-Gómez, R., Salgado-Garciglia, R., Ochoa-Zarzosa, A. and López-Meza, J.E. (2018) PaDef Defensin from Avocado (Persea Americana var. Drymifolia) Is Cytotoxic to K562 Chronic Myeloid Leukemia Cells through Extrinsic Apoptosis. *The International Journal of Biochemistry & Cell Biology*, **99**, 10-18. https://doi.org/10.1016/j.biocel.2018.03.013

[10] Jiménez-Alcántar, P., López-Gómez, R., López-Meza, J.E. and Ochoa-Zarzosa, A. (2022) PaDef (Persea Americana var. Drymifolia), a Plant Antimicrobial Peptide, Triggers Apoptosis, and Induces Global Epigenetic Modifications on Histone 3 in an Acute Lymphoid Leukemia Cell Line. *Frontiers in Molecular Biosciences*, **9**, Article ID: 801816. https://doi.org/10.3389/fmolb.2022.801816

[11] Salvesen, G.S., Hempel, A. and Coll, N.S. (2015) Protease Signaling in Animal and Plant-Regulated Cell Death. *The FEBS Journal*, **283**, 2577-2598. https://doi.org/10.1111/febs.13616

[12] Tsiatsiani, L. and Heck, A.J.R. (2015) Proteomics Beyond Trypsin. *The FEBS Journal*, **282**, 2612-2626. https://doi.org/10.1111/febs.13287

[13] Clemente, M., Corigliano, M.G., Pariani, S.A., Sánchez-López, E.F., Sander, V.A. and Ramos-Duarte, V.A. (2019) Plant Serine Protease Inhibitors: Biotechnology Application in Agriculture and Molecular Farming. *International Journal of Molecular Sciences*, **20**, Article 1345. https://doi.org/10.3390/ijms20061345

[14] Antão, C.M. and Malcata, F.X. (2005) Plant Serine Proteases: Biochemical, Physiological and Molecular Features. *Plant Physiology and Biochemistry*, **43**, 637-650. https://doi.org/10.1016/j.plaphy.2005.05.001

[15] Hedstrom, L. (2002) Serine Protease Mechanism and Specificity. *Chemical Reviews*, **102**, 4501-4524. https://doi.org/10.1021/cr000033x

[16] Craik, C.S., Page, M.J. and Madison, E.L. (2011) Proteases as Therapeutics. *Biochem-*

ical Journal, **435**, 1-16. https://doi.org/10.1042/bj20100965

[17] Bitoun, E., Chavanas, S., Irvine, A.D., Lonie, L., Bodemer, C., Paradisi, M., *et al*. (2002) Netherton Syndrome: Disease Expression and Spectrum of SPINK5 Mutations in 21 Families. *Journal of Investigative Dermatology*, **118**, 352-361. https://doi.org/10.1046/j.1523-1747.2002.01603.x

[18] Ritchie, B.C. (2003) Protease Inhibitors in the Treatment of Hereditary Angioedema. *Transfusion and Apheresis Science*, **29**, 259-267. https://doi.org/10.1016/j.transci.2003.08.004

[19] Qi, R., Song, Z. and Chi, C. (2005) Structural Features and Molecular Evolution of Bowman-Birk Protease Inhibitors and Their Potential Application. *Acta Biochimica et Biophysica Sinica*, **37**, 283-292. https://doi.org/10.1111/j.1745-7270.2005.00048.x

[20] Daliri, E., Oh, D. and Lee, B. (2017) Bioactive Peptides. *Foods*, **6**, Article 32. https://doi.org/10.3390/foods6050032

[21] Abdel-Magid, A.F. (2015) Allosteric Modulators: An Emerging Concept in Drug Discovery. *ACS Medicinal Chemistry Letters*, **6**, 104-107. https://doi.org/10.1021/ml5005365

[22] Erlanger, B.F., Kokowsky, N. and Cohen, W. (1961) The Preparation and Properties of Two New Chromogenic Substrates of Trypsin. *Archives of Biochemistry and Biophysics*, **95**, 271-278. https://doi.org/10.1016/0003-9861(61)90145-x

[23] Pliego-Arreaga, R., Roldán-Padrón, O., Castro-Guillén, J.L., Mendiola-Olaya, E., Jiménez-Sandoval, P., Brieba, L.G., *et al*. (2019) Properties of a Non-Canonical Complex Formed between a Tepary Bean (*Phaseolus acutifolius*) Protease Inhibitor and A-chymotrypsin. *The Protein Journal*, **38**, 435-446. https://doi.org/10.1007/s10930-019-09863-2

[24] Waterhouse, A., Bertoni, M., Bienert, S., Studer, G., Tauriello, G., Gumienny, R., *et al*. (2018) SWISS-MODEL: Homology Modelling of Protein Structures and Complexes. *Nucleic Acids Research*, **46**, W296-W303. https://doi.org/10.1093/nar/gky427

[25] Gasteiger, E., Hoogland, C., Gattiker, A., Duvaud, S., Wilkins, M.R., Appel, R.D., *et al*. (2005) Protein Identification and Analysis Tools on the Expasy Server. In: Walker, J.M., Ed., *The Proteomics Protocols Handbook*, Humana Press, 571-607. https://doi.org/10.1385/1-59259-890-0:571

[26] Berman, H.M. (2000) The Protein Data Bank. *Nucleic Acids Research*, **28**, 235-242. https://doi.org/10.1093/nar/28.1.235

[27] Pettersen, E.F., Goddard, T.D., Huang, C.C., Couch, G.S., Greenblatt, D.M., Meng, E.C., *et al*. (2004) UCSF Chimera—A Visualization System for Exploratory Research and Analysis. *Journal of Computational Chemistry*, **25**, 1605-1612. https://doi.org/10.1002/jcc.20084

[28] Morris, G.M., Huey, R., Lindstrom, W., Sanner, M.F., Belew, R.K., Goodsell, D.S., *et al*. (2009) Autodock4 and Autodocktools4: Automated Docking with Selective Receptor Flexibility. *Journal of Computational Chemistry*, **30**, 2785-2791. https://doi.org/10.1002/jcc.21256

[29] Zhang, Y. and Sanner, M.F. (2019) *Autodock crankpep*: Combining Folding and Docking to Predict Protein-Peptide Complexes. *Bioinformatics*, **35**, 5121-5127. https://doi.org/10.1093/bioinformatics/btz459

[30] BIOVIA (2019) Dassault Systèmes BIOVIA, Discovery Studio Modeling Environment. Dassault Systèmes.

[31] Phillips, J.C., Hardy, D.J., Maia, J.D.C., Stone, J.E., Ribeiro, J.V., Bernardi, R.C., *et al*. (2020) Scalable Molecular Dynamics on CPU and GPU Architectures with NAMD.

The Journal of Chemical Physics, **153**, Article 044130. https://doi.org/10.1063/5.0014475

[32] Jo, S., Kim, T., Iyer, V.G. and Im, W. (2008) CHARMM-GUI: A Web-Based Graphical User Interface for CHARMM. *Journal of Computational Chemistry*, **29**, 1859-1865. https://doi.org/10.1002/jcc.20945

[33] Kim, S., Lee, J., Jo, S., Brooks, C.L., Lee, H.S. and Im, W. (2017) CHARMM-GUI Ligand Reader and Modeler for CHARMM Force Field Generation of Small Molecules. *Journal of Computational Chemistry*, **38**, 1879-1886. https://doi.org/10.1002/jcc.24829

[34] Jorgensen, W.L., Chandrasekhar, J., Madura, J.D., Impey, R.W. and Klein, M.L. (1983) Comparison of Simple Potential Functions for Simulating Liquid Water. *The Journal of Chemical Physics*, **79**, 926-935. https://doi.org/10.1063/1.445869

[35] Huang, J., Rauscher, S., Nawrocki, G., Ran, T., Feig, M., de Groot, B.L., *et al*. (2016) Charmm36m: An Improved Force Field for Folded and Intrinsically Disordered Proteins. *Nature Methods*, **14**, 71-73. https://doi.org/10.1038/nmeth.4067

[36] Essmann, U., Perera, L., Berkowitz, M.L., Darden, T., Lee, H. and Pedersen, L.G. (1995) A Smooth Particle Mesh Ewald Method. *The Journal of Chemical Physics*, **103**, 8577-8593. https://doi.org/10.1063/1.470117

[37] Fletcher, R. and Reeves, C.M. (1964) Function Minimization by Conjugate Gradients. *The Computer Journal*, **7**, 149-154. https://doi.org/10.1093/comjnl/7.2.149

[38] Feller, S.E., Zhang, Y., Pastor, R.W. and Brooks, B.R. (1995) Constant Pressure Molecular Dynamics Simulation: The Langevin Piston Method. *The Journal of Chemical Physics*, **103**, 4613-4621. https://doi.org/10.1063/1.470648

[39] Martyna, G.J., Hughes, A. and Tuckerman, M.E. (1999) Molecular Dynamics Algorithms for Path Integrals at Constant Pressure. *The Journal of Chemical Physics*, **110**, 3275-3290. https://doi.org/10.1063/1.478193

[40] Humphrey, W., Dalke, A. and Schulten, K. (1996) VMD: Visual Molecular Dynamics. *Journal of Molecular Graphics*, **14**, 33-38. https://doi.org/10.1016/0263-7855(96)00018-5

[41] Genheden, S. and Ryde, U. (2015) The MM/PBSA and MM/GBSA Methods to Estimate Ligand-Binding Affinities. *Expert Opinion on Drug Discovery*, **10**, 449-461. https://doi.org/10.1517/17460441.2015.1032936

[42] Weng, G., Wang, E., Chen, F., Sun, H., Wang, Z. and Hou, T. (2019) Assessing the Performance of MM/PBSA and MM/GBSA Methods. 9. Prediction Reliability of Binding Affinities and Binding Poses for Protein-Peptide Complexes. *Physical Chemistry Chemical Physics*, **21**, 10135-10145. https://doi.org/10.1039/c9cp01674k

[43] Valdés-Tresanco, M.S., Valdés-Tresanco, M.E., Valiente, P.A. and Moreno, E. (2021) Gmx_MMPBSA: A New Tool to Perform End-State Free Energy Calculations with GROMACS. *Journal of Chemical Theory and Computation*, **17**, 6281-6291. https://doi.org/10.1021/acs.jctc.1c00645

[44] Parekh, V.J., Rathod, V.K. and Pandit, A.B. (2011) Substrate Hydrolysis: Methods, Mechanism, and Industrial Applications of Substrate Hydrolysis. In: Moo-Young, M., Ed., *Comprehensive Biotechnology*, Elsevier, 103-118. https://doi.org/10.1016/b978-0-08-088504-9.00094-5

[45] Polgár, L. (2005) The Catalytic Triad of Serine Peptidases. *Cellular and Molecular Life Sciences*, **62**, 2161-2172. https://doi.org/10.1007/s00018-005-5160-x

[46] Baird, T.T., Wright, W.D. and Craik, C.S. (2006) Conversion of Trypsin to a Functional Threonine Protease. *Protein Science*, **15**, 1229-1238.

https://doi.org/10.1110/ps.062179006

[47] George, R.A., Spriggs, R.V., Bartlett, G.J., Gutteridge, A., MacArthur, M.W., Porter, C.T., *et al*. (2005) Effective Function Annotation through Catalytic Residue Conservation. *Proceedings of the National Academy of Sciences*, **102**, 12299-12304. https://doi.org/10.1073/pnas.0504833102

[48] Stewart, K.D., Bentley, J.A. and Cory, M. (1990) Docking Ligands into Receptors: The Test Case of A-Chymotrypsin. *Tetrahedron Computer Methodology*, **3**, 713-722. https://doi.org/10.1016/0898-5529(90)90169-9

[49] Gul, S. and Khan, A.M. (2022) Molecular Docking Studies of Isolated Marine Natural Products against A-Chymotrypsin. *Natural Product Research*, **38**, 1269-1272. https://doi.org/10.1080/14786419.2022.2132501

[50] Erlanger, B.F., Wassermann, N.H. and Cooper, A.G. (1973) Allosteric Activation of Chymotrypsin-Catalyzed Hydrolysis of Specific Substrates. *Biochemical and Biophysical Research Communications*, **52**, 208-215. https://doi.org/10.1016/0006-291x(73)90975-3

[51] Erlanger, B.F., Wassermann, N.H., Cooper, A.G. and Monk, R.J. (1976) Allosteric Activation of the Hydrolysis of Specific Substrates by Chymotrypsin. *European Journal of Biochemistry*, **61**, 287-295. https://doi.org/10.1111/j.1432-1033.1976.tb10021.x

[52] Tomassen, M.M.M., Barrett, D.M., van der Valk, H.C.P.M. and Woltering, E.J. (2007) Isolation and Characterization of a Tomato Non-Specific Lipid Transfer Protein Involved in Polygalacturonase-Mediated Pectin Degradation. *Journal of Experimental Botany*, **58**, 1151-1160. https://doi.org/10.1093/jxb/erl288

[53] Melo, F.R., Rigden, D.J., Franco, O.L., Mello, L.V., Ary, M.B., Grossi de Sá, M.F., *et al*. (2002) Inhibition of Trypsin by Cowpea Thionin: Characterization, Molecular Modeling, and Docking. *Proteins*: *Structure*, *Function*, *and Bioinformatics*, **48**, 311-319. https://doi.org/10.1002/prot.10142

Supplementary Material

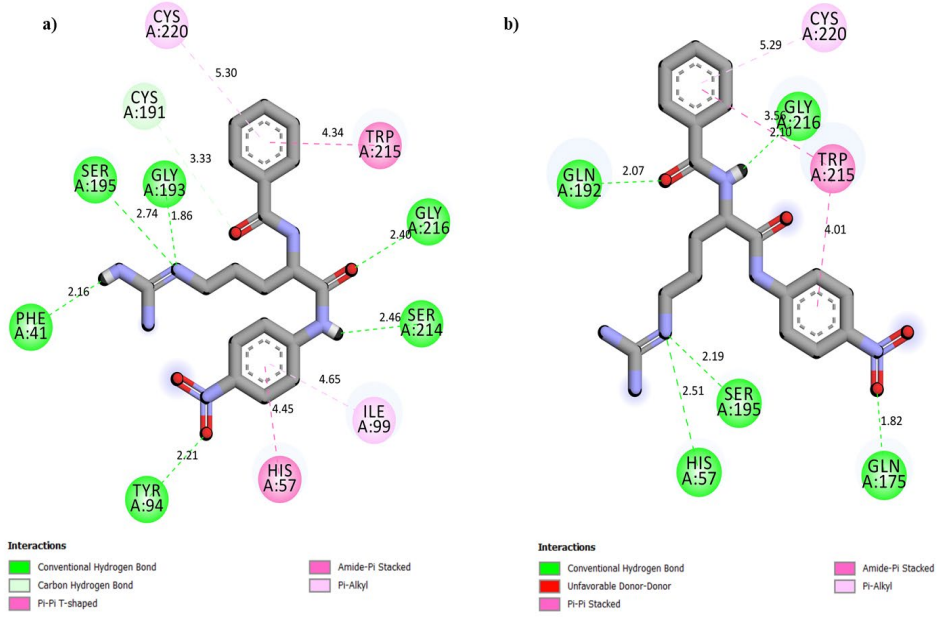

Figure S1. Interactions and distances (in Å), between the BApNA against (a) Chymotrypsin A (C) and (b) Trypsin (T) in the catalytic region.

Table S1. Intermolecular interactions (in Å), donor and acceptor residues between peptide 1 (p1) against Chymotrypsin A (C) in the catalytic region.

Type	Distance	Donor-Acceptor	
Salt Bridge	2.49	p1:LYS8:N	C:ASP64:O
Hydrogen Bond	3.26	C:GLY193:N	p1:GLU4:O
Hydrogen Bond	3.09	C:SER195:N	p1:GLU4:O
Hydrogen Bond	2.64	C:SER195:O	p1:GLU4:O
Hydrogen Bond	3.02	C:GLY216:N	p1:THR2:O
Hydrogen Bond	3.32	C:GLY216:N	p1:THR2:O
Hydrogen Bond	2.47	p1:THR2:O	C:GLY216:O
Hydrogen Bond	2.64	p1:THR5:O	C:PHE41:O
Hydrogen Bond	2.71	p1:THR5:O	C:CYS42:S
Hydrogen Bond	2.91	p1:PHE10:N	C:ASP35:O
C-H	3.13	C:SER190:C	p1:GLU4:O
π-Cation	4.12	C:LYS36:N	p1:PHE10
π-Cation	4.29	p1:LYS8:N	C:PHE41
π-σ	3.71	p1:LYS8:C	C:PHE41
π-Sulfur	3.61	p1:CYS3:S	C:HIS57
π-π Stacked	4.26	p1:HIS9	C:PHE39
Alkyl	4.86	p1:CYS3	C:ILE99
π-Alkyl	4.90	p1:PHE10	C:LYS36

Table S2. Intermolecular interactions (in Å), donor and acceptor residues between peptide 1 (p1) against Chymotrypsin A (C) found near the alternative region 1.

Type	Distance	Donor-Acceptor	
Salt Bridge	3.09	C:ARG145:N	p1:GLU4:O
Attractive Charge	2.54	p1:LYS8:N	C:GLU20:O
Hydrogen Bond	2.89	C:ASN18:N	p1:THR2:O
Hydrogen Bond	2.65	C:ASN18:N	p1:CYS3:O
Hydrogen Bond	2.95	C:GLU21:N	p1:LYS8:O
Hydrogen Bond	3.04	C:THR144:O	p1:PHE10:O
Hydrogen Bond	2.92	C:THR222:O	p1:THR2:O
Hydrogen Bond	2.91	p1:LYS8:N	C:SER11:O
Hydrogen Bond	3.16	p1:PHE10:N	C:GLN156:O
C-H	3.48	p1:LYS8:C	C:GLU21:O
C-H	2.79	p1:HIS9:C	C:GLN156:O
π-Alkyl	5.12	C:TYR146	p1:ALA1
π-Alkyl	5.29	p1:PHE10	C:ARG154
Unfavorable Donor-Donor	3.04	C:TYR146:N	p1:ALA1:N

Table S3. Intermolecular interactions (in Å), donor and acceptor residues between peptide 1 (p1) against Chymotrypsin A (C) found near the alternative region 2.

Type	Distance	Donor-Acceptor	
Salt Bridge	2.72	p1:LYS8:N	C:ASP129:O
Attractive Charge	2.81	C:LYS202:N	p1:GLU4:O
Hydrogen Bond	2.84	C:LEU10:N	p1:CYS3:O
Hydrogen Bond	3.27	C:THR135:N	p1:PRO6:O
Hydrogen Bond	2.26	p1:THR2:O	C:PRO8:O
Hydrogen Bond	2.91	p1:SER7:O	C:THR135:O
C-H	3.05	p1:SER7:C	C:LYS202:O
π-Donor Hydrogen Bond	3.11	C:ASP129:N	p1:PHE10
Alkyl	4.49	C:ALA131	p1:LYS8
Alkyl	5.48	p1:CYS3	C:LEU10
Unfavorable Bump	2.40	C:LEU10:O	p1:CYS3:S
Unfavorable Acceptor-Acceptor	2.75	C:THR135:O	p1:PRO6:O

Table S4. Intermolecular interactions (in Å), donor and acceptor residues between peptide 2 (p2) against Chymotrypsin A (C) in the catalytic region.

Type	Distance	Donor-Acceptor	
Attractive Charge	3.61	C:LYS170:N	P2:GLU17:O
Hydrogen Bond	3.27	C:TYR171:O	P2:ALA11:O
Hydrogen Bond	2.55	C:TYR171:O	P2:VAL13:O
Hydrogen Bond	2.48	C:SER195:O	P2:GLY2:O

Continued

Hydrogen Bond	2.48	C:SER217:O	P2:SER12:O
Hydrogen Bond	2.63	C:SER218:N	P2:SER12:O
Hydrogen Bond	2.60	C:SER218:O	P2:SER8:O
Hydrogen Bond	2.69	C:THR219:N	P2:SER12:O
Hydrogen Bond	2.85	P2:ASN1:N	C:HIS57:O
Hydrogen Bond	2.55	P2:ASN1:N	C:CYS58:O
Hydrogen Bond	2.76	P2:ASN9:N	C:TYR146:O
Hydrogen Bond	3.15	P2:ASN9:N	C:SER218:O
Hydrogen Bond	2.66	P2:GLU17:N	C:LYS170:O
Hydrogen Bond	2.85	P2:HIS18:N	C:LYS170:O
C-H	3.36	C:TRP215:C	P2:LEU3:O
C-H	3.17	C:SER218:C	P2:ASN9:O
C-H	3.13	P2:LEU3:C	C:SER195:O
C-H	3.67	P2:PHE19:C	C:ASN167:O
Alkyl	3.77	C:ILE99	P2:ILE5
Alkyl	5.13	P2:CYS4	C:MET192
π-Alkyl	4.52	C:HIS57	P2:ILE5
π-Alkyl	5.20	C:TRP172	P2:ALA11
π-Alkyl	4.92	P2:PHE19	C:LEU163

Table S5. Intermolecular interactions (in Å), donor and acceptor residues between peptide 2 (p2) against Chymotrypsin A (C) found near the alternative region 1.

Type	Distance	Donor-Acceptor	
Salt Bridge	2.47	p2:ARG6:N	C:ASP153:O
Attractive Charge	5.40	C:ARG145:N	p2:GLU17:O
Attractive Charge	5.23	C:ARG145:N	p2:GLU17:O
Hydrogen Bond	2.70	C:ASN18:N	p2:HIS15:O
Hydrogen Bond	3.45	C:GLY19:N	p2:CYS14:S
Hydrogen Bond	3.14	C:ILE80:N	p2:ASN1:O
Hydrogen Bond	2.92	C:THR144:N	p2:SER12:O
Hydrogen Bond	2.87	C:ASN150:N	p2:CYS10:O
Hydrogen Bond	2.91	C:THR222:N	p2:HIS18:O
Hydrogen Bond	2.70	p2:ILE5:N	C:THR37:O
Hydrogen Bond	2.69	p2:ARG6:N	C:THR151:O
Hydrogen Bond	2.88	p2:ARG6:N	C:THR151:O
Hydrogen Bond	2.55	p2:ASN9:N	C:ASP153:O
Hydrogen Bond	2.55	p2:ASN9:N	C:ASP153:O
Hydrogen Bond	3.56	p2:CYS14:S	C:GLY19:O
C-H	3.28	p2:ARG6:C	C:GLN73:O
C-H	2.91	p2:SER12:C	C:ASN150:O

Continued

C-H	3.05	p2:CYS14:C	C:THR144:O
C-H	3.42	p2:HIS18:C	C:THR222:O
C-H	3.56	p2:HIS18:C	C:THR222:O
π-Donor Hydrogen Bond	3.44	C:THR219:O	p2:PHE19
π-σ	3.50	C:VAL17:C	p2:HIS15
π-Alkyl	4.42	p2:HIS15	C:ARG145
Unfavorable Bump; Hydrogen Bond	2.21	C:THR144:O	p2:SER12:O
Unfavorable Positive-Positive	5.16	C:LYS82:N	p2:ASN1:N
Unfavorable Donor-Donor	2.84	C:ASN150:N	p2:CYS10:N

Table S6. Intermolecular interactions (in Å), donor and acceptor residues between peptide 2 (p2) against Chymotrypsin A (C) found near the alternative region 2.

Type	Distance	Donor-Acceptor	
Salt Bridge	2.61	p2:ARG6:N	C:GLU78:O
Attractive Charge	2.74	C:LYS202:N	p2:GLU17:O
Attractive Charge	5.47	p2:ARG6:N	C:ASP72:O
Hydrogen Bond	3.40	C:GLN116:N	p2:CYS4:S
Hydrogen Bond	2.36	C:THR117:O	p2:LEU3:O
Hydrogen Bond	3.06	p2:ASN1:N	C:SER113:O
Hydrogen Bond	2.50	p2:ASN1:N	C:PHE114:O
Hydrogen Bond	2.83	p2:SER7:O	C:GLN116:O
Hydrogen Bond	2.72	p2:ASN9:N	C:GLN7:O
Hydrogen Bond	2.57	p2:GLY16:N	C:LEU10:O
Hydrogen Bond	3.02	p2:GLU17:N	C:LEU10:O
π-σ	3.87	C:THR135:C	p2:HIS18
π-Lone Pair	2.99	C:THR135:O	p2:HIS18
π-π T-shaped	4.89	p2:HIS18	C:TRP207
Alkyl	4.09	C:LYS79	p2:ILE5
Alkyl	5.31	C:VAL118	p2:LEU3
Alkyl	4.95	p2:ARG6	C:PRO24
Alkyl	4.66	p2:CYS10	C:VAL9
Alkyl	4.10	p2:ALA11	C:VAL23
Alkyl	5.03	p2:ALA11	C:PRO24
π-Alkyl	5.35	p2:HIS18	C:VAL137
π-Alkyl	4.53	p2:PHE19	C:LYS202
Unfavorable Donor-Donor	2.81	C:GLN7:N	p2:ASN9:N

Table S7. Intermolecular interactions (in Å), donor and acceptor residues between peptide 3 (p3) against Chymotrypsin A (C) in the catalytic region.

Type	Distance	Donor-Acceptor	
Salt Bridge	2.90	p3:ARG9:N	C:ASP64:O
Salt Bridge	2.70	p3:ARG10:N	C:ASP35:O
Salt Bridge	3.27	p3:LYS16:N	C:ASP35:O
Attractive Charge	4.87	p3:ARG9:N	C:ASP64:O
Attractive Charge	4.84	p3:ARG10:N	C:ASP35:O
Hydrogen Bond	3.11	C:SER195:O	p3:GLN6:O
Hydrogen Bond	2.67	C:SER218:O	p3:ASP2:O
Hydrogen Bond	3.03	C:SER218:O	p3:ASP2:O
Hydrogen Bond	2.94	p3:ASP2:N	C:SER218:O
Hydrogen Bond	2.78	p3:ARG4:N	C:SER96:O
Hydrogen Bond	2.44	p3:ARG4:N	C:LEU97:O
Hydrogen Bond	3.01	p3:ARG9:N	C:GLY59:O
Hydrogen Bond	2.54	p3:ARG11:N	C:HIS40:O
π-Cation	3.39	p3:ARG9:N	C:PHE41
π-Cation	4.80	p3:ARG10:N	C:PHE39
Alkyl	4.67	p3:CYS5	C:MET192
Alkyl	5.28	p3:ARG11	C:MET192
Alkyl	5.26	p3:CYS18	C:LYS36
π-Alkyl	5.18	C:PHE39	p3:ARG10
π-Alkyl	4.70	C:PHE39	p3:CYS12
π-Alkyl	4.93	C:PHE41	p3:ARG9

Table S8. Intermolecular interactions (in Å), donor and acceptor residues between peptide 3 (p3) against Chymotrypsin A (C) found near the alternative region 1.

Type	Distance	Donor-acceptor	
Salt Bridge	2.99	C:ARG145:N	p3:ASP2:O
Salt Bridge	3.86	p3:ARG4:N	C:GLU20:O
Salt Bridge	3.21	p3:ARG9:N	C:GLU21:O
Salt Bridge	2.84	p3:ARG9:N	C:GLU21:O
Salt Bridge	2.73	p3:ARG10:N	C:ASP72:O
Attractive Charge	5.18	C:ARG145:N	p3:ASP2:O
Attractive Charge	5.03	p3:ARG10:N	C:ASP72:O
Attractive Charge	4.65	p3:ARG10:N	C:ASP153:O
Attractive Charge	4.37	p3:LYS16:N	C:ASP153:O
Hydrogen Bond	2.76	C:ASN18:N	p3:THR1:O
Hydrogen Bond	3.02	C:GLU21:N	p3:GLN6:O
Hydrogen Bond	3.17	C:THR37:O	p3:CYS18:S
Hydrogen Bond	2.97	C:THR144:O	p3:ASP2:O

Continued

Hydrogen Bond	2.83	C:ASN150:N	p3:MET13:O
Hydrogen Bond	3.05	C:ARG154:N	p3:GLY7:O
Hydrogen Bond	3.12	C:GLN156:N	p3:GLN6:O
Hydrogen Bond	2.98	p3:ARG4:N	C:ASN18:O
Hydrogen Bond	3.38	p3:LEU15:N	C:ASP153:O
Hydrogen Bond	2.93	p3:LYS16:N	C:GLN73:O
Hydrogen Bond	3.12	p3:CYS18:S	C:THR37:O
C-H	3.73	p3:PRO17:C	C:GLN73:O
Alkyl	5.27	C:PRO152	p3:MET13
Unfavorable Bump; Hydrogen Bond	2.17	p3:ARG4:N	C:GLY19:O
Unfavorable Donor-Donor	3.08	C:ASN18:N	p3:GLY3:N
Unfavorable Donor-Donor	3.11	C:ARG154:N	p3:ARG10:N
Unfavorable Acceptor-Acceptor	2.47	C:GLU21:O	p3:GLN6:O

Table S9. Intermolecular interactions (in Å), donor and acceptor residues between peptide 3 (p3) against Chymotrypsin A (C) found near the alternative region 2.

Type	Distance	Donor-acceptor	
Salt Bridge	2.46	p3:ARG11:N	C:GLU20:O
Attractive Charge	3.76	C:ARG145:N	p3:ASP2:O
Hydrogen Bond	2.84	C:ASN18:N	p3:GLN6:O
Hydrogen Bond	3.31	C:SER159:N	p3:CYS12:S
Hydrogen Bond	2.88	C:THR222:N	p3:CYS5:O
Hydrogen Bond	2.66	p3:CYS5:S	C:THR219:O
Hydrogen Bond	3.09	p3:CYS5:S	C:CYS220:O
Hydrogen Bond	2.48	p3:GLY7:N	C:THR222:O
Hydrogen Bond	2.83	p3:VAL8:N	C:THR222:O
Hydrogen Bond	2.86	p3:ARG10:N	C:SER186:O
C-H	2.96	C:SER221:C	p3:CYS5:O
C-H	3.68	p3:CYS12:C	C:SER159:O
C-H	2.90	p3:PRO17:C	C:LEU10:O
Alkyl	4.99	C:VAL9	p3:PRO17
Alkyl	4.75	C:PRO161	p3:MET13
Alkyl	4.84	p3:CYS12	C:LEU10
Alkyl	4.75	p3:CYS14	C:LEU10

Table S10. Intermolecular interactions (in Å), donor and acceptor residues between peptide 4 (p4) against Trypsin (T) in the catalytic region.

Type	Distance	Donor-acceptor	
Hydrogen Bond	2.13	T:HIS57:H	p4:GLU4:O
Hydrogen Bond	2.69	T:LYS60:H	p4:CYS3:S
Hydrogen Bond	2.45	T:TYR151:H	p4:GLU4:O

Continued

Hydrogen Bond	1.98	T:GLN192:H	p4:THR5:O
Hydrogen Bond	1.78	T:GLY216:H	p4:PRO6:O
Hydrogen Bond	2.29	T:GLY219:H	p4:SER7:O
Hydrogen Bond	2.87	p4:THR2:N	T:HIS57:O
Hydrogen Bond	2.69	p4:THR2:O	T:HIS57:O
Hydrogen Bond	3.04	p4:THR5:O	T:CYS191:O
Hydrogen Bond	2.71	p4:THR5:O	T:SER195:O
Hydrogen Bond	3.22	p4:LYS8:N	T:ASN97:O
C-H	3.77	T:HIS57:C	p4:THR2:O
C-H	2.74	T:HIS57:C	p4:THR2:O
C-H	3.59	T:CYS58:C	p4:THR2:O
C-H	2.91	p4:PRO6:C	T:SER214:O
C-H	2.66	p4:SER7:C	T:GLY216:O
π-σ	3.50	p4:LYS8:C	T:TRP215
π-Sulfur	5.64	p4:CYS3:S	T:TYR39
Alkyl	4.91	p4:ALA1	T:LYS60
Alkyl	4.71	p4:PRO6	T:LEU99
π-Alkyl	4.88	T:PHE41	p4:CYS3
π-Alkyl	3.94	T:HIS57	p4:PRO6
π-Alkyl	4.72	T:TRP215	p4:LYS8
Unfavorable Acceptor-Acceptor	2.88	T:HIS57:O	p4:THR2:O

Table S11. Intermolecular interactions (in Å), donor and acceptor residues between peptide 5 (p5) against Trypsin (T) in the catalytic region.

Type	Distance	Donor-acceptor	
Salt Bridge	3.08	p5:ARG8:N	T:ASP153:O
Attractive Charge	4.73	p5:ARG8:N	T:ASP153:O
Hydrogen Bond	2.80	T:ASN74:H	p5:CYS6:O
Hydrogen Bond	1.85	T:GLY193:H	p5:PHE2:O
Hydrogen Bond	3.14	p5:HIS1:N	T:SER195:O
Hydrogen Bond	3.08	p5:HIS1:N	T:GLY219:O
Hydrogen Bond	3.66	p5:HIS1:N	T:CYS220:S
Hydrogen Bond	2.96	p5:ASN3:N	T:HIS57:O
Hydrogen Bond	3.21	p5:GLY4:N	T:PHE41:O
Hydrogen Bond	3.13	p5:CYS6:N	T:HIS40:O
Hydrogen Bond	3.08	p5:CYS6:S	T:PRO152:O
Hydrogen Bond	2.66	p5:ARG8:N	T:ASP153:O
Hydrogen Bond	2.51	p5:ARG8:N	T:TYR151:O
C-H	2.76	T:PHE41:C	p5:GLY4:O
C-H	3.47	T:HIS57:C	p5:ASN3:O

Continued

C-H	3.52	T:CYS58:C	p5:ASN3:O
C-H	3.36	T:TRP215:C	p5:HIS1:O
C-H	3.33	T:GLY226:C	p5:HIS1:N
C-H	2.92	p5:HIS1:C	T:ASP189:O
C-H	3.08	p5:LEU5:C	T:HIS40:O
Sulfur-X	2.72	T:CYS42:S	p5:ASN3:O
π-σ	3.56	p5:LEU5:C	T:TYR39
π-Sulfur	4.77	T:CYS220:S	p5:HIS1
Alkyl	4.59	p5:CYS6	T:ILE73
π-Alkyl	5.10	T:HIS40	p5:CYS6
π-Alkyl	5.48	T:TYR151	p5:CYS6

Table S12. Intermolecular interactions (in Å), donor and acceptor residues between peptide 6 (p6) against Trypsin (T) in the catalytic region.

Type	Distance	Donor-acceptor	
Salt Bridge; Attractive Charge	2.03	T:LYS60:H	p6:GLU11:O
Salt Bridge	2.97	p6:ARG17:N	T:ASP153:O
Attractive Charge	3.63	T:HIS40:N	p6:ASP15:O
Hydrogen Bond	2.10	T:SER96:H	p6:SER6:O
Hydrogen Bond	2.28	T:SER96:H	p6:SER6:O
Hydrogen Bond	2.48	p6:SER2:O	T:PRO92:O
Hydrogen Bond	2.79	p6:ASN3:N	T:PRO92:O
Hydrogen Bond	2.44	p6:ASN3:N	T:TYR94:O
Hydrogen Bond	2.91	p6:CYS4:N	T:PRO92:O
Hydrogen Bond	3.62	p6:CYS4:S	T:VAL90:O
Hydrogen Bond	3.05	p6:SER6:O	T:SER96:O
Hydrogen Bond	2.63	p6:GLY10:N	T:TYR59:O
Hydrogen Bond	3.02	p6:HIS12:N	T:HIS57:O
Hydrogen Bond	3.18	p6:ARG17:N	T:TRP141:O
Hydrogen Bond	2.72	p6:ARG17:N	T:PRO152:O
Hydrogen Bond	2.84	p6:ARG17:N	T:PRO152:O
C-H	3.15	T:HIS40:C	p6:ASP15:O
C-H	3.13	T:GLY193:C	p6:ASP15:O
C-H	3.54	p6:SER6:C	T:TYR94:O
π-Cation	4.19	T:HIS57:N	p6:PHE13
π-σ	2.98	T:HIS57:C	p6:HIS12
π-π T-shaped	5.02	T:HIS57	p6:PHE13
Alkyl	4.08	T:VAL90	p6:VAL7
Alkyl	4.37	p6:CYS4	T:VAL90
π-Alkyl	4.55	T:TYR94	p6:VAL7
π-Alkyl	4.69	T:TYR151	p6:ARG17
Unfavorable Donor-Donor	3.40	T:ASN74:H	p6:ARG17:N

Table S13. Intermolecular interactions (in Å), donor and acceptor residues between peptide 7 (p7) against Trypsin (T) in the catalytic region.

Type	Distance	Donor-acceptor	
Attractive Charge	4.91	p7:CYS1:N	T:ASP189:O
Attractive Charge	5.44	p7:CYS1:N	T:ASP194:O
Hydrogen Bond	2.75	T:TYR39:H	p7:ARG5:O
Hydrogen Bond	2.16	T:LYS60:H	p7:ARG5:O
Hydrogen Bond	1.99	T:GLN192:H	p7:GLN2:O
Hydrogen Bond	2.36	T:GLY193:H	p7:GLY3:O
Hydrogen Bond	3.04	T:SER195:H	p7:GLY3:O
Hydrogen Bond	3.52	p7:CYS1:S	T:ASP189:O
Hydrogen Bond	3.72	p7:CYS1:S	T:SER190:O
Hydrogen Bond	3.10	p7:CYS1:S	T:GLY219:O
Hydrogen Bond	2.52	p7:GLN2:N	T:GLY216:O
Hydrogen Bond	3.20	p7:ARG5:N	T:PHE41:O
C-H	3.44	p7:VAL4:C	T:PHE41:O
π-Cation	4.08	p7:ARG5:N	T:TYR151
Alkyl	4.05	T:CYS42	p7:VAL4
Alkyl	4.35	T:CYS58	p7:VAL4
π-Alkyl	5.46	T:PHE41	p7:VAL4
π-Alkyl	5.48	T:HIS57	p7:VAL4
Unfavorable Bump	1.99	T:GLY216:N	p7:GLN2:O
Unfavorable Bump; Hydrogen Bond	1.25	T:GLY216:H	p7:GLN2:O
Unfavorable Donor-Donor	2.67	T:HIS57:H	p7:GLY3:N
Unfavorable Donor-Donor	2.26	T:SER195:H	p7:GLY3:N

Table S14. Intermolecular interactions (in Å), donor and acceptor residues between peptide 8 (p8) against Trypsin (T) in the catalytic region.

Type	Distance	Donor-acceptor	
Salt Bridge; Attractive Charge	2.16	p8:ARG2:H	T:ASP189:O
Salt Bridge; Attractive Charge	2.07	p8:ARG2:H	T:ASP189:O
Attractive Charge	4.92	T:HIS57:N	p8:ARG2:O
Attractive Charge	4.17	p8:ARG2:N	T:ASP189:O
Hydrogen Bond	2.25	T:HIS57:H	p8:ARG2:O
Hydrogen Bond	2.75	T:GLN192:H	p8:ARG1:O
Hydrogen Bond	2.39	T:GLY193:H	p8:ARG2:O
Hydrogen Bond	2.16	p8:ARG1:H	T:GLY216:O
Hydrogen Bond	2.12	p8:ARG1:H	T:GLY216:O
Hydrogen Bond	1.87	p8:ARG1:H	T:SER96:O
Hydrogen Bond	2.37	p8:ARG1:H	T:ASN97:O
Hydrogen Bond	2.36	p8:ARG1:H	T:ASN97:O

Continued

Hydrogen Bond	1.95	p8:ARG1:H	T:SER96:O
Hydrogen Bond	1.91	p8:ARG2:H	T:SER190:O
Hydrogen Bond	3.06	p8:ARG2:H	T:SER190:O
Hydrogen Bond	1.84	p8:ARG2:H	T:GLY219:O
C-H	2.89	T:GLN192:C	p8:ARG2:O
Unfavorable Positive-Positive	3.05	T:HIS57:N	p8:ARG2:O
Unfavorable Donor-Donor	1.88	T:GLY216:H	p8:ARG1:H
Unfavorable Acceptor-Acceptor	2.90	T:GLY216:O	p8:ARG1:O

Table S15. Intermolecular interactions (in Å), donor and acceptor residues between peptide 9 (p9) against Trypsin (T) in the catalytic region.

Type	Distance	Donor-acceptor	
Attractive Charge	4.88	p9:LYS5:N	T:ASP189:O
Hydrogen Bond	2.00	T:TYR39:H	p9:CYS1:O
Hydrogen Bond	2.35	T:HIS57:H	p9:LEU4:O
Hydrogen Bond	1.76	T:LYS60:H	p9:CYS1:O
Hydrogen Bond	2.08	T:GLN192:H	p9:LYS5:O
Hydrogen Bond	1.83	T:GLY216:H	p9:PRO6:O
Hydrogen Bond	2.46	T:GLY219:H	p9:CYS7:S
Hydrogen Bond	3.09	A p9:CYS3:N	T:PHE41:O
Hydrogen Bond	2.89	p9:LYS5:N	T:GLY219:O
C-H	3.44	T:SER195:C	p9:CYS3:O
C-H	3.68	p9:LYS5:C	T:SER190:O
C-H	2.60	p9:PRO6:C	T:SER214:O
Alkyl	3.97	T:CYS42	p9:CYS3
Alkyl	3.86	T:CYS58	p9:CYS3
Alkyl	4.57	p9:PRO6	T:LEU99
π-Alkyl	5.10	T:TYR39	p9:MET2
π-Alkyl	4.86	T:PHE41	p9:CYS3
π-Alkyl	4.11	T:HIS57	p9:PRO6
Unfavorable Positive-Positive	4.39	T:LYS60:N	p9:CYS1:N
Unfavorable Donor-Donor	2.56	T:TYR39:H	p9:CYS1:N
Unfavorable Donor-Donor	3.27	T:GLY193:H	p9:LYS5:N
Unfavorable Acceptor-Acceptor	2.61	T:GLY216:O	p9:PRO6:O